

# Fine Robotic Manipulation without Force/Torque Sensor

Shilin Shan<sup>1,\*</sup> and Quang-Cuong Pham<sup>2</sup>

**Abstract**—Force Sensing and Force Control are essential to many industrial applications. Typically, a 6-axis Force/Torque (F/T) sensor is mounted between the robot’s wrist and the end-effector in order to measure the forces and torques exerted by the environment onto the robot (the external wrench). Although a typical 6-axis F/T sensor can provide highly accurate measurements, it is expensive and vulnerable to drift and external impacts. Existing methods aiming at estimating the external wrench using only the robot’s internal signals are limited in scope: for example, wrench estimation accuracy was mostly validated in free-space motions and simple contacts as opposed to tasks like assembly that require high-precision force control. Here we present a Neural Network based method and argue that by devoting particular attention to the training data structure, it is possible to accurately estimate the external wrench in a wide range of scenarios based solely on internal signals. As an illustration, we demonstrate a pin insertion experiment with 100-micron clearance and a hand-guiding experiment, both performed without external F/T sensors or joint torque sensors. Our result opens the possibility of equipping the existing 2.7 million industrial robots with Force Sensing and Force Control capabilities without any additional hardware.

**Index Terms**—External Wrench Estimation, Machine Learning, Mechanisms Modeling & Control, Human-robot Interaction

## I. INTRODUCTION

Force Sensing and Force Control are essential to many industrial applications, from contact-based inspection to assembly, sanding, deburring, and polishing [1]–[3]. Typically, a 6-axis Force/Torque (F/T) sensor is mounted between the robot’s wrist and the end-effector in order to measure the forces and torques exerted by the environment onto the robot (the external wrench). Although a typical 6-axis F/T sensor can provide highly accurate measurements, it is expensive and vulnerable to drift and external impacts. Consequently, there has been a significant research effort aimed at estimating the external wrench using only the robot’s internal signals, such as joint position, joint velocity, or motor current readings.

To that aim, there are two main approaches in the literature: model-based and model-free. In the model-based approach, parameterized models of the robot’s dynamics are developed and identified using standard parameter identification techniques [4]–[7]. The main difficulty here lies in the accurate and reliable modeling and identification of highly nonlinear,

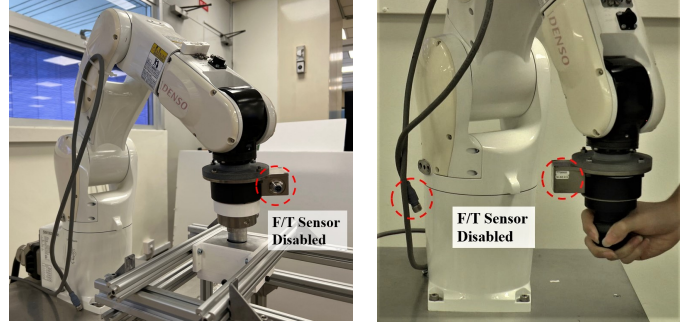


Fig. 1: Snapshot of the sensorless tight pin insertion and hand-guiding experiment setup. Video demonstrations of the experiments in Section V is available in the supplementary materials or at: [https://youtu.be/04\\_f3coFzaQ](https://youtu.be/04_f3coFzaQ)

nonsmooth phenomena such as hysteresis and joint friction. Model-free methods, based, e.g., on Neural Networks, have been developed to overcome this difficulty [8]–[10]. However, such methods have been so far limited in scope: for example, wrench estimation accuracy was mostly validated in free-space motions and simple contacts as opposed to complex industrial tasks that require high-precision force control.

In general, to our knowledge, no method – whether model-based or model-free – has been shown to accurately and reliably estimate the external wrench in both free-space and in-contact motions. This requirement is crucial for achieving non-trivial tasks like tight assembly and hand-guiding, alternating between free-space and in-contact robot motions. These tasks have yet to be demonstrated in existing works and are, more generally, necessary for large-scale industrial deployment.

Here we present a model-free method (based on Neural Networks) and argue that the above requirement can be satisfied if particular attention is devoted to the structure of the training dataset. In particular, we highlight the importance of collecting training data for both free-space and in-contact motions. Doing so enables us to accurately and reliably estimate external wrench using only internal signals such as joint position, velocity, acceleration, and current readings.

More specifically,

- We propose a pure Neural Network based method that takes joint currents and states as input and returns the end-effector wrench. The Neural Network maps the input variables needed for a dynamic model to the output wrench directly, so no additional Dynamic Model identification and joint torque sensing are required. In addition, the use of joint current allows wrench estimation without

<sup>1</sup> Shilin Shan is with School of Mechanical and Aerospace Engineering, Nanyang Technological University, Singapore (address: 50 Nanyang Ave, Singapore 639798; phone: +65 6790 5568; e-mail: shilin.shan153@gmail.com)

<sup>2</sup> Quang-Cuong Pham is with Eureka Robotics and Singapore Centre for 3D Printing (SC3DP), School of Mechanical and Aerospace Engineering, Nanyang Technological University, Singapore. (e-mail: cuong@ntu.edu.sg)

\* Corresponding author: Shilin Shan

the embedded joint torque sensors, which reduces robot manufacturing costs.

- We present a pipeline that collects data automatically and efficiently in wrench estimation problems by emphasizing the data collection procedure. The training data was collected with not only the free-space trajectories but also constrained in-contact motions so as to induce disturbances that create more variability in the data set. The trained model has high accuracy in typical industrial tasks like tight pin insertion and high-precision hand-guiding, which, to our knowledge, have yet to be demonstrated with the existing methods.

As an illustration, we demonstrate the pin insertion experiment with 100-micron clearance and the hand-guiding experiment, both performed without F/T sensors at runtime. Note that a 6-axis F/T sensor would be needed for the one-time data collection on a single manipulator in the training phase. For large-scale industrial applications, a well-trained Neural Network can be applied to any manipulators of the same model, either manufactured or to be manufactured, to equip them with force/torque sensing ability without physical sensors.

The paper is organized as follows. In Section II, we discuss the literature on wrench estimation and dynamics identification. In Section III, we present the basic model structure and the concepts for data sets generation. In Section IV, we discuss in detail the data collection procedure and model enhancement approaches for broader work-space coverage. In Section V, we present four experiments in free-space and in-contact scenarios to demonstrate the robustness of the proposed method. Fig. 1 shows a snapshot of the sensorless pin insertion and hand-guiding experiments.

## II. RELATED WORK

Previous works on contact detection [4], [11] introduced using the generalized momentum to identify the Inverse Dynamic Model, and a generalized-momentum-based disturbance observer is designed in [5]. By integrating with the Kalman Filter, the combined approach [6] allows accurate force estimation that can be used for basic force control tasks. The author also addressed that joint friction, an essential component in dynamic modeling, can be calculated by considering Coulomb friction, viscous friction, stiction, and Stribeck velocity. Earlier studies [12]–[14] have also shown that non-linear behaviors like hysteresis and back-lashes can be well identified, thus compensated by such a modeling method. On the other hand, deciding the friction model parameters may require complex experiments.

Although mathematical analysis provides strong intuitions to the robot dynamics, identifying the Inverse Dynamic Model through mathematical analysis of mechanical models is still complicated. In order to simplify modeling complexity, recent studies have proposed semi-parametric approaches to train Neural Network models to learn joint motor friction [15] or compensate for all the non-modeled effects [16]. Given that parameter identifications are still required for rigid body dynamics, these methods reduce only modeling complexity, whereas even more experiments would be needed to learn a friction model separately.

Another approach is to avoid manually selecting the whole model structure and make the model learn through one-time data collection. Non-parametric regression-based approaches have been studied for model identification in early research [17], [18]. Multiple studies have built on these methods and demonstrated the ease of training of non-parametric learning-based approaches, including Gaussian Process Regression (GPR) and Locally Weighted Projection Regression (LWPR) [8], [9], [19]. Without choosing the model structure manually, regression-based approaches avoid human bias on the model structure, thus allowing a model to learn the optimal structure given simple hyper-parameters. Being trained and verified with hand-guiding experiments [9], GPR shows high accuracy in hand-guided trajectory tracking. However, trajectory tracking only is not representative of various industrial tasks. Furthermore, this method may not be transferable to other tasks; as discussed in Section III, the hand-guiding data set could be biased due to the strong correlation between the end-effector force and motion.

Following Section I, we propose to use Neural Networks, particularly Multilayer Perceptron (MLP), to avoid complex mathematical modeling while ensuring estimation accuracy, as it has been proven effective in approximating nonlinear mapping in many areas. Also discussed in [20], Neural Networks performed well in approximating the forward/inverse kinematics, and Jacobian matrix [21]–[23]. Recent works have proposed a variety of Neural Network structures, including MLP [24], Recurrent Neural Network (RNN) [25], and Convolutional Neural Network (CNN) [26]–[28], being applied in different tasks. Though demonstrating promising results, the works mentioned above are hard to compare as they were implemented in a very different context that requires image input or surgical robot setup. Some closely related applications of MLP in industrial manipulator collision checking can be found in [10], [29], where models are trained to predict external torque for threshold determination or directly detect contact during motions. Even though Neural Network is less intuitive in revealing robot dynamics, it generally outperforms most methods in nonlinear mapping and noise cancellation, thereby being robust in uncertain environments given sufficient training data.

## III. MODEL AND TRAINING SET STRUCTURE

### A. Model Structure

Given the broad application of Neural Networks in regression problems for robotics, multiple structures, i.e., MLP, RNN, CNN, have been proposed for similar tasks as discussed above. Considering model simplicity and ease of implementation, we choose the model to have a fundamental MLP structure with only a few hidden layers. As shown in the experiments, since MLP already shows high accuracy in multiple tasks, we will not discuss the use of more complex structures like CNN and RNN in this paper. On the other hand, when a simple model covers a large joint-space or work-space, it will underfit the training data such that estimation becomes inaccurate. Our solution is to enlarge the hidden layers or increase Network depth to capture higher non-linearity and

diversities introduced by dissimilar Inverse Kinematics Classes (IK Classes for short). Therefore, a model should be retrained and optimized whenever new data is collected from distal IK Classes. A detailed discussion of the relationship between the model and data size is included in Section IV.

Fig. 2 helps to visualize a sample model structure with two hidden layers, each having 256 neurons. The input to the Neural Network is a  $24 \times 1$  vector that concatenates the  $6 \times 1$  joint current,  $6 \times 1$  joint position,  $6 \times 1$  joint velocity, and  $6 \times 1$  joint acceleration vector. The model output is a  $6 \times 1$  vector consisting of the  $3 \times 1$  force vector and  $3 \times 1$  torque vector in the XYZ direction, all represented in the F/T Sensor (end-effector) frame. We implemented the model and data loader, then trained the model with PyTorch. The loss function, activation function, and optimization method are MSEloss, ReLu, and Adam Optimizer, respectively.

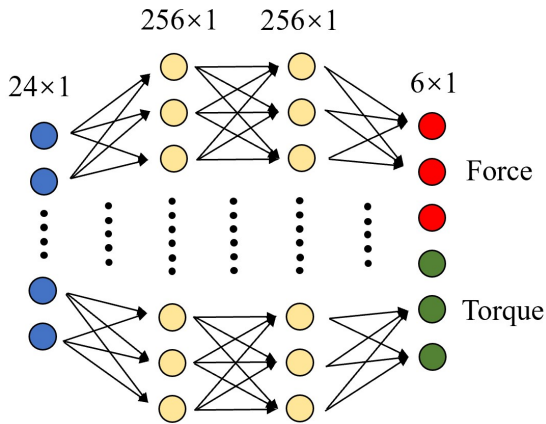


Fig. 2: Structure of the proposed MLP model

### B. Training Set Structure

The training set consists of two data set: Free-space Data Set and Contact Data Set.

The Free-space Data Set (FSDS) was collected when the robot end-effector followed pre-planned trajectories. FSDS aims to train the Neural Network for the essential force/torque sensing ability, so it includes random contact, measured by an F/T Sensor, at the end-effector throughout data collection. It is the training set's fundamental component, or backbone, for it can provide a model with some basic information about the robot. With only FSDS, a model is expected to estimate wrench accurately within the work-space for data collection regardless of motion complexity. In other words, the robot can achieve simple tasks like contact detection after being trained by FSDS.

The Contact Data Set (CDS) is useful in fine-tuning and enhancing a model's performance in more complex scenarios. The robot joints' states, currents, and external forces/torques vibrate at high frequencies in force control tasks, such as constrained sliding on a plane and pin insertion. The resulting controlled trajectories that the end-effector follows are not pre-planned smooth trajectories but real-time evaluated trajectories with many uncertainties. Therefore, CDS trains the model to

make clear estimations even though joint currents and states are noisy.

We distinguish and identify FSDS and CDS as the backbone and fine-tuning data sets for the reason that CDS may teach the model biased information about the robot dynamics. During FSDS collection, all trajectories are pre-determined, and end-effector forces are random, suggesting that the instantaneous end-effector motion, and thereby joint states, are uncorrelated with the wrench. In contrast, in contact tasks, the end-effector always moves in directions minimizing contact force error. For sliding motions, the friction force is always opposite to the motion parallel to contact planes. A worse scenario could be hand-guiding, where end-effector motion is always compliant with force and torque. Therefore, our concern is that CDS from a specific task may reduce accuracy for other tasks. Although such a phenomenon is not obvious in the experiments, where one fine-tuned model by hand-guiding data set can still be used for in-contact sliding, discriminating against the biased information hopefully ensures the desired outcome.

## IV. TRAINING SET COLLECTION AND MODEL TRAINING

Data collection and experiments demonstrated in the next section were carried out on Denso-VS060, a 6-axis industrial robot. We used Ubuntu and Robot Operating System (ROS) for hardware interface, robot motion planning, and joint current and state extraction. An ATI Gamma F/T Sensor SI-32-2.5 was used for force control and simultaneously training data collection. The CPU model was: Intel(R) Xeon(R) CPU E5-2630 v3 @ 2.40GHz, and the additional computational resources (four GPUs) involved in Neural Network training were of the type: GeForce GTX 1080 Ti. Data loading and training typically take 10 minutes with the above device specifications and the following training data size. There was no GPU used to assist in real-time wrench estimation.

The end-effector for FSDS collection was a 3D-printed sphere with 50mm diameter, which allowed easy grasping and twisting. The end-effector for CDS collection was an aluminum cylinder pin with 20mm diameter. Both end-effectors were mounted directly on the F/T Sensor.

### A. Training Sets Generation

1) *Free-space Data Set (FSDS)*: FSDS was collected when the robot end-effector followed randomized trajectories in a cuboid work-space. To begin with, multiple end-effector positions were randomly generated in sequence inside the work-space. Each point was assigned a rotation matrix for the end-effector, with Euler angles  $\theta_x$ ,  $\theta_y$ , and  $\theta_z$  randomly selected from the specified ranges. Afterward, a trajectory planner explored every point in sequence and planned the shortest trajectory from one point to the next. Data was collected by randomly applying forces on the end-effector manually and continuously when it followed the pre-planned trajectories. A position-controlled robot was used for experiments, so its joint velocity and acceleration were calculated through the first and second derivatives of joint position. Although current and acceleration signals were very noisy, the input to the model was not filtered as we expect a short estimation delay and that the

model may eliminate the effect of noise through learning. The real-time Force/Torque Sensor reading, joint current, position, velocity, and acceleration were simultaneously recorded as the training data at 100HZ.

2) *Contact Data Set (CDS)*: We collected the preliminary CDS through direct end-effector contact with planes to introduce less data bias and train a model that can accomplish most of the experiments designed in section V. The data set was collected when the end-effector made contact and slid on a steel plate with controlled contact force. With the plate location fixed inside the work-space for FSDS, multiple contact points were generated in sequence in the specified rectangular region on the plate. The end-effector repeated the following for each contact point: (1) Making contact with the plate at a random angle, then pushing the plate with a reference force for 30 seconds. In order to induce disturbances, a random reference force was sampled within the range [4N, 30N] every 0.2s. (2) Sliding towards the next contact point while maintaining the force. (3) Leaving off the plate after reaching the next point. Similarly, the real-time Force/Torque Sensor reading and joint states were recorded simultaneously at 100HZ throughout the steps above.

As shown in Fig. 5a, contact force was controlled through end-effector position control in the corresponding direction. The F/T Sensor feedback error was passed to a P controller to decide the displacement perpendicular to the plate. Sliding motions parallel to the plate followed the pre-planned straight trajectories between points, so sliding friction was not controlled. Using the Inverse Kinematics Model, we can evaluate the commanded joint positions and send them to the robot with the desired X, Y, and Z coordinates.

CDS collection should repeat for multiple contact planes so that CDS covers a possibly large portion of the work-space. However, this may require a flexible experiment setup where the plane location and orientation are adjustable. The ideal data collection setup for commercialization and large-scale deployment would have two robots pushing against each other to simulate in-contact effects. Optionally, the contact plate could be mounted to the robot’s end-effector so that the plane locations and trajectories are programmable. Due to the setup constraint, we collect CDS on two contact planes with three different IK Classes.

### B. Training Set Details

We collected three data sets, each including both FSDS and CDS, with three IK Classes. The exact work-space size and location, contact plane size and location, and total data frames can be found in Table I. Fig. 3 helps to visualize these regions and the corresponding IK Classes in OpenRave simulated environment. Training data distributions, particularly joint position and velocity distribution, are shown in Appendix Fig. A.1 in histograms.

### C. Model Enhancement for Large Work-space

It is validated in the literature of deep learning [30] that MLP has the potential to fit any non-linear equations given

IK Class 1		
Space Size (m) $0.20 \times 0.50 \times 0.15$	Space Center (m) [0.35, 0.00, 0.30]	FSDS Frames 991,500
Plane Size (m) Horizontal $0.15 \times 0.20$	Plane Center (m) [0.35, -0.14, 0.30]	CDS Frames 1,653,000
IK Class 2		
Space Size (m) $0.25 \times 0.20 \times 0.40$	Space Center (m) [0.40, 0.15, 0.60]	FSDS Frames 1,098,500
Plane Size (m) Vertical $0.20 \times 0.30$	Plane Center (m) [0.40, 0.20, 0.60]	CDS Frames 2,635,000
IK Class 3		
Space Size (m) $0.20 \times 0.20 \times 0.20$	Space Center (m) [0.35, 0.15, 0.65]	FSDS Frames 825,500
Plane Size (m) Vertical $0.15 \times 0.20$	Plane Center (m) [0.37, 0.20, 0.65]	CDS Frames 1,686,500

TABLE I: The work-space specifications, plane specifications, and training data size for three data sets. Coordinates are represented in the robot base frame.

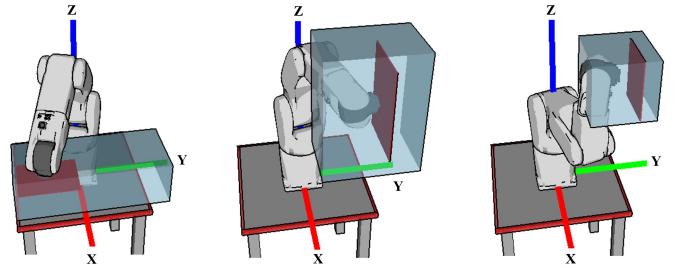


Fig. 3: Visualization of the data region for three work-spaces with three different IK Classes. The transparent blue box and opaque red plane indicate the bounding boxes and location of the fixed plates, respectively. The postures of Denso from left to right show the center of the nearest joint position clusters, or IK solutions, based on which the data was collected.

appropriate model structure and sufficient training data. However, a learning-based model generally loses accuracy when covering data with higher non-linearity. This phenomenon is obvious whenever new training data is collected from different joint specifications and distal IK Classes. An intuitive solution is increasing the model size, that is, adding more hidden layers or neurons. On the other hand, instantaneous wrench feedbacks are crucial in real-time tasks, especially high-precision force-control tasks like assembly. A large model will lead to a long inference time given a general industrial application scenario, where additional computational resources like GPUs are costly. Therefore, a tradeoff between model size and inference time must be made according to the expected model performance in applications.

In order to optimize the model structure for experiments, we train models of three different hidden layer sizes (LS) with either single or entire data sets coverage, then compare the RMSE of all wrench dimensions on the same test set (150,000 frames). All models have the same depth of two hidden layers. The numerical results are shown in Table II. Estimation accuracy generally increases for all dimensions as we enlarge hidden layers, but inference time increases from 0.05ms for LS128 to 0.20ms for LS256 and 0.80ms for LS512 in our implementation. It is also clear that the accuracy of a smaller model drops significantly when covering three

data sets, but it is not obvious for larger models. Estimation accuracy and inference time should be tested carefully when larger models or data sets are desired.

It was observed that the training data down-sampled by five times trained the model for a similar estimation accuracy, but the training set with four-fifths of the trajectory removed resulted in poor accuracy. This suggests that the coverage of trajectories and their complexities dominate the model accuracy instead of simply the training data size. Hopefully, estimation accuracy can be improved further if the training set trajectories are optimized.

LS	Datasets	Test Set RMSE (N for F; Nm for T)					
		Fx	Fy	Fz	Tx	Ty	Tz
128	1	4.08	3.84	5.23	0.24	0.25	0.08
256	1	3.45	3.35	4.50	0.22	0.23	0.08
512	1	2.70	2.96	4.04	0.18	0.18	0.08
128	1,2,3	5.62	5.29	6.90	0.33	0.36	0.11
256	1,2,3	3.91	3.71	5.23	0.26	0.27	0.09
512	1,2,3	3.11	2.99	4.43	0.22	0.20	0.08

TABLE II: RMSE on the same test set (randomly sampled from data set 1) produced by models with different hidden layer size (LS) and training data coverage. Fx, Fy, and Fz stands for end-effector forces in XYZ directions. Tx, Ty, and Tz stands for end-effector torques in XYZ directions.

## V. EXPERIMENT RESULTS

### A. Wrench Estimation in Free Motion

Given that the model with 512 hidden neurons has a relatively high accuracy while the inference time is less than 1 ms in our implementation, we use this structure for all experiments presented in the following sections.

The free-motion experiment served as a online test set for the trained model. Test trajectories were generated randomly in the same manner as the FSDS collection in the work-space for IK Class 1. When the robot was executing, periodical forces and torques were applied to a spherical end-effector mounted on the F/T sensor. Fig. 4 shows a comparison between a part of the real-time estimated wrench and the real-time reading from the Force/Torque sensor when the end-effector followed pre-planned free-space trajectories. RMSEs in this and all the remaining experiments are calculated regarding the data presented in figures. The plot suggests that although the model missed some peak values, it can still follow the overall wrench variation despite random end-effector trajectories. The magnitude of RMSE is also acceptable, considering the force/torque variation ranges.

### B. Force Control For In-contact Spiral Sliding

The end-effector followed a pre-planned spiral trajectory with the fixed plate location. Similarly, force control was achieved through position control as suggested in Fig. 5a, but we used the estimated result from the Neural Network Estimator to replace the F/T sensor for control feedback. That means that the contact force was controlled with real-time estimated force with a simple P controller. Fig. 5b shows the block diagram for closed-loop control of contact force.

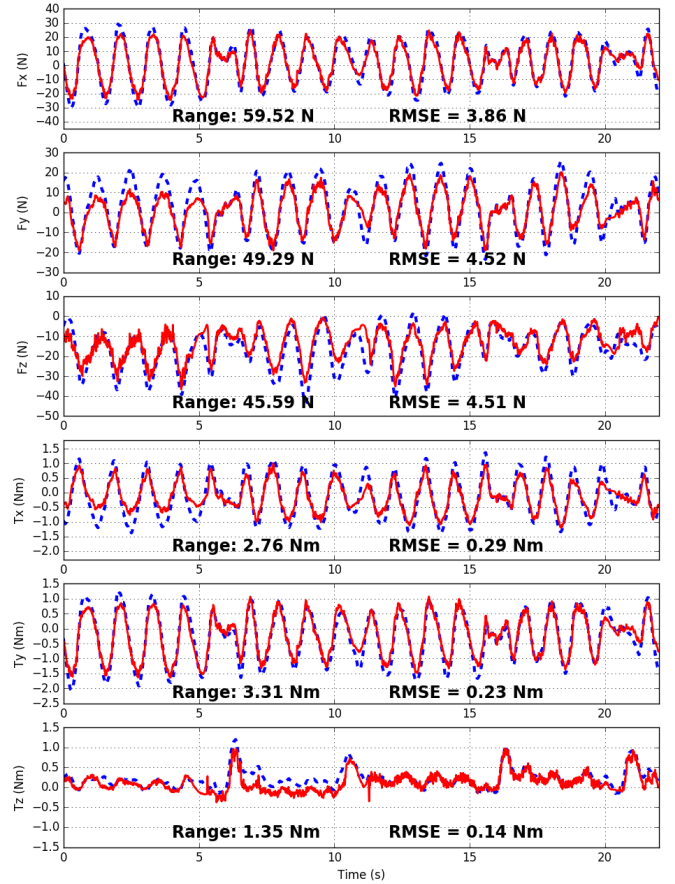


Fig. 4: Comparison between the estimated (red) and real wrench (blue dashed) for random pre-planned free-motion trajectories. Forces and torque are represented in the F/T Sensor (end-effector) frame.

In the experiment, the end-effector first moved towards the plate, then tried to apply a constant force of 15N with a contact angle of  $10^\circ$ , and finally started sliding following a spiral trajectory after the force was stabilized. The plate location is the same as that for data collection with IK Class 1. Fig. 6 compares the estimated wrench and sensor reading during sliding. The effect of force control can be interpreted from the force along the Z-axis. It is obvious that forces and torques parallel to the plate undergo sinusoidal variation due to the periodic friction change during spiral sliding. Although spiral trajectories are excluded from the training set, the model can still perform accurate wrench estimation learning from simple straight motions. Again, neither the input data to nor output data from the model were filtered. The estimated wrench is noisy due to the unprocessed input and simple controller, but the overall accuracy is promising.

### C. Force/Torque Control for Tight Assembly

In addition to the contact force control task, a strong proof of the estimator's reliability is completing a typical industrial task - tight assembly. In the general scenario of pin insertion, forces and torques in all directions are under control, so the

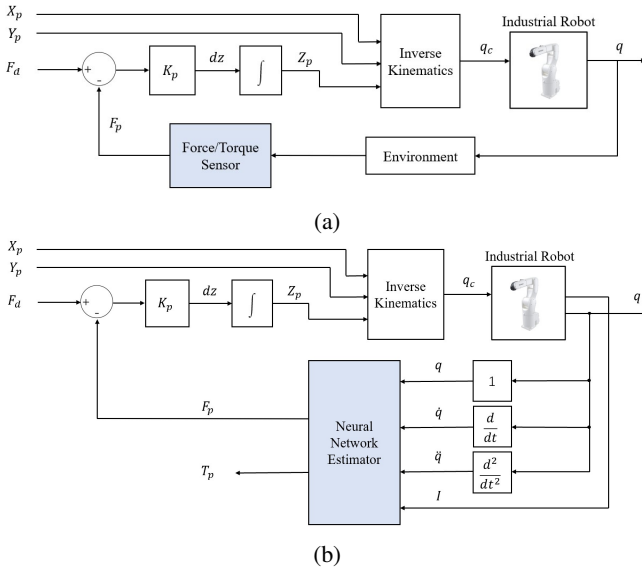


Fig. 5: (a) Block diagram for force control on contact planes.  $X_p$ ,  $Y_p$ , and  $Z_p$  are the end-effector coordinate in the plate's frame.  $F_d$  is the desired force on the plate.  $F_p$  is the force perpendicular to the plate evaluated from the F/T sensor measurement. (b) Block diagram for force control on planes with Neural Network estimation.  $I$  indicates the joint current.

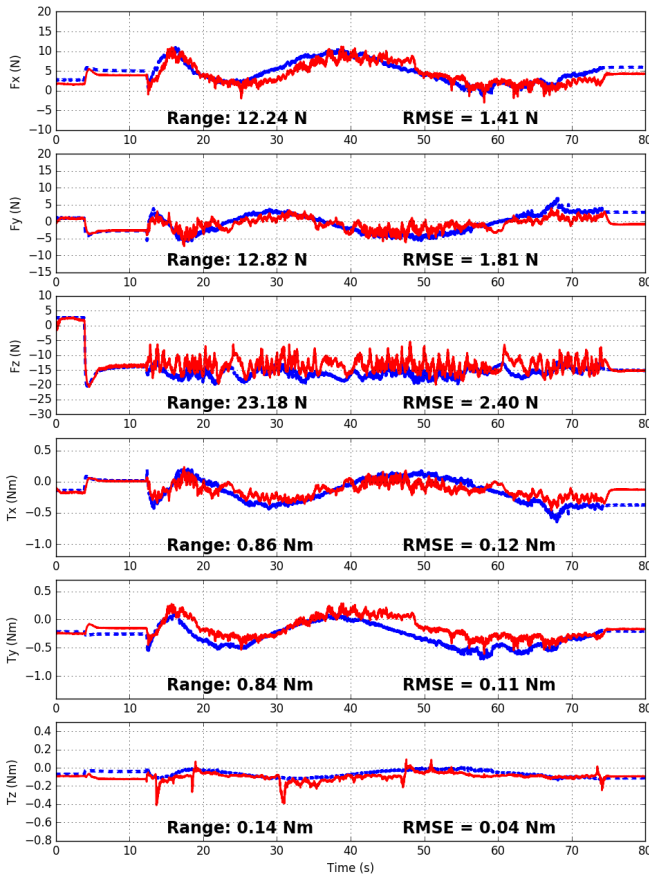


Fig. 6: Comparison between the estimated (red) and real wrench (blue dashed) for in-contact spiral sliding. Forces and torque are represented in the F/T Sensor (end-effector) frame.

task requires high force-sensing accuracy with only a slight lag in time.

In this experiment, we used one pair of aluminum pin and hole with 20mm diameters and 100-micron clearance. In the force-controlled insertion, the hole was placed in the work-space for IK Class 1, and the pin was mounted on the F/T sensor (for comparison purposes only) through coupling. Insertion started 3mm above the hole with 2mm horizontal position error and  $5^\circ$  orientation error. Again, the estimated wrench was used as the control feedback, and the control algorithm for pin insertion was designed as follows: (1) forces and torques were transformed into the pin-tip frame; (2) [0N, 0N, 10N, 0Nm, 0Nm] reference force and torque were used as the controller setpoint (end-effector twist not controlled). The algorithm results in a three-phase insertion as shown in Fig. 7, where the pin moved downward before making contact, automatically located and aligned with the hole while maintaining the contact force, and finally fitted into the hole after being aligned. Note that the relative initial orientation error of the pin and hole was roughly  $5^\circ$ , but the hole's orientation was assumed unknown. Torque control was thus needed to align the pin and hole while locating the hole center.

During insertion, the pin made multiple-point contact with the hole as a need for torque control. It was observed that torques being transmitted to joints are different with the same torque on the sensor in the multiple-point and single-point contact scenario, such that joint current measurements are different. It suggests that one joint current reading may correspond to two different end-effector torque under single-point and multiple-point contact, given some robot configurations. Such a phenomenon is always true at specific configurations like wrist singularity. Even with the robot being close to those configurations, the model trained with noisy data still cannot capture the slight current changes. As a result, in the insertion experiment, torque estimation was relatively accurate in the first 5 seconds when the pin made single-point contact with the hole. However, the model failed to estimate torque accurately in the complex multiple-contact part and stuck with only 12mm inserted. Minimum pin-insertion training data was then collected to allow full insertion of 18mm.

Fig. 8 shows the comparison between the estimated and true wrench for the whole insertion process. However, torque estimation for multiple-point contact is still inaccurate, as explained above, even though the pin was successfully inserted. The accuracy may be improved by including more complex motions and force control tasks in the training set. Another approach could be manipulating and training the model with the residual between the measured and estimated free-space current instead so that the model learns for slight current variations more effectively.

#### D. Sensorless Hand-guiding

With hand-guiding, a typical human-robot interaction task, we demonstrate how the model can be fine-tuned for different tasks by the corresponding data set. As discussed in Section III, the hand-guiding data set was not used for backbone training with concern that the end-effector and joint motions

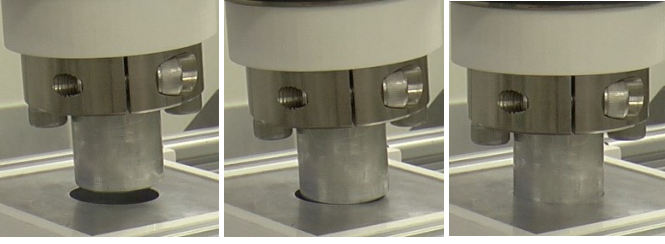


Fig. 7: Three-phase insertion procedure governed by  $[0\text{N}, 0\text{N}, 10\text{N}, 0\text{Nm}, 0\text{Nm}]$  reference forces and torques. In phase one, the pin moved to the hole until making contact with  $10\text{N}$  reference force. In phase two, it rotated to align with the hole and automatically located the hole center due to zero reference forces and torques except for the Z direction. In phase three, the pin was aligned, and thus inserted further.

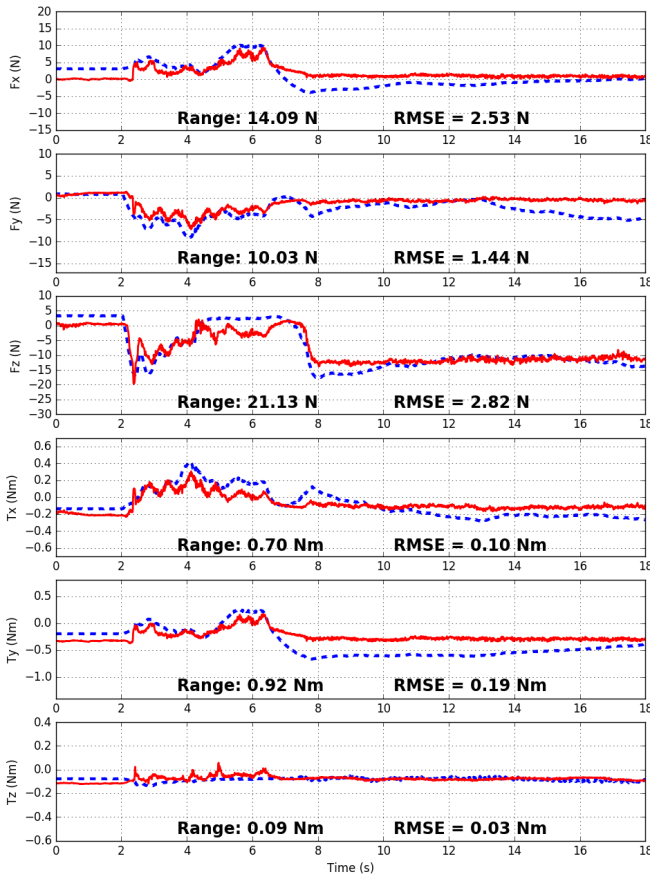


Fig. 8: Comparison between the estimated (red) and real wrench (blue dashed) in force/torque controlled pin insertion task. Forces and torque are represented in the F/T Sensor (end-effector) frame.

are always compliant with forces. The compliant motion could generate biased data with which the Neural Network may underfit the actual dynamics. In other words, the forces and robot motions strongly correlate due to hand-guiding.

The hand-guiding data set includes 321,000 data frames collected with IK Class 1 recorded at  $100\text{Hz}$ . The end-effector, the same as that for FSDS collection, was guided to follow

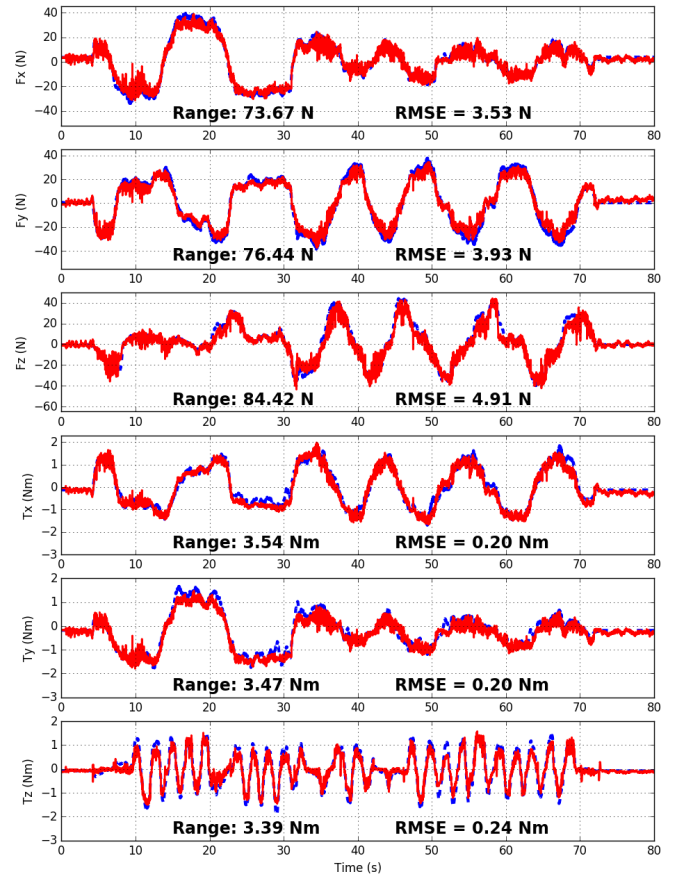


Fig. 9: Comparison between the estimated (red) and real wrench (blue dashed) in hand-guiding. Forces and torque are represented in the F/T Sensor (end-effector) frame.

straight and spiral trajectories that explore the pre-defined work-space. Again, we used a simple P controller for data collection, then trained the model with unprocessed data to ensure that it learned in a noisy environment. The fine-tuned model was then tested in the same work-space. A part of the record is shown in Fig. 9. With the almost overlapped estimation with the ground-truth, we conclude that the Neural Network estimator has great potential to be used for various tasks through fine-tuning. Even though the estimated wrench was noisy due to the discontinuous trajectory, the stability could be improved with further signal processing.

#### E. Error Quantification in the Frequency Domain

Considering the complex environment in which a robot could operate, studying the model behavior under different contact force frequencies is crucial. More specifically, we studied the estimation error and phase lag as a function of force oscillation frequency. Data was collected in the work-space for IK Class 1 with the same plate location for training data collection. Ten contact points were evenly sampled on the plate, and for each point, the end-effector oscillated between two reference positions penetrating into the plane. The exact penetration depths were determined through preliminary experiments, so the resulting force vibration had an identical

mean and range of 15N and 10N for all frequencies. Note that direct force control was not applied as the oscillation range shrank significantly at higher frequencies even though the reference force is unchanged. Data were recorded at multiple frequencies from 0.1Hz to 10Hz for each contact point, and 645,500 data frames were recorded in total.

Although RMSE is intuitive and widely used for error analysis, our experiments show that RMSE from the same model can vary depending on the force variation range. It can be interpreted easily by comparing Fig. 8 and Fig. 9, where the latter plot looks more accurate intuitively but actually has larger errors. Normalized RMSE could be a better choice, but selecting the appropriate lower and upper bound for normalization still depends on the force range required in different tasks. Therefore, we quantify the estimation error as the ratio and offset between the estimated force and the true force in the same frame. More specifically, we used linear regression to obtain a first-order approximation of the mapping from the true force to the estimated force in each frequency. The physical meaning for ratio and offset is the magnitude gain from the true to estimated force and the mean error between the forces, respectively.

With the direct position-control pattern, as shown in Fig. 10, the estimated force tends to overshoot after reaching the desired position, and that is caused by the overshoot in motor current. Higher frequencies do not allow the current to stabilize, such that the overshoot error dominates as frequency increases. Such an interpretation can be visualized in Fig. 11, where both the gain and offset have a local maximum at 1Hz oscillation. When frequency increases further, the overshoot would be eliminated, so the local minimum at 3Hz suggests the overall accuracy in an overshoot-free and marginally stable condition. Oscillation becomes irregular after 3Hz, with shrinking oscillation ranges and non-identical current behaviors in each period. Such chaotic behavior, though similar to that in most industrial applications, makes it hard to analyze intuitively, but both the ratio and offset stay in reasonable ranges. The RMSE plot suggests that the absolute error is roughly 2N with a 15N and 10N force oscillation mean and range. By calculating the cross-correlation of the estimation and measurement data series, there is no apparent relationship found between time lead or lag and oscillation frequency.

## VI. CONCLUSION

In this paper, we propose an approach to estimating the end-effector wrench with Neural Networks. The model takes the joint currents and states as the input and makes estimations of the wrench in real-time. It avoids using embedded joint torque sensors and can replace 6-axis end-effector F/T sensors in industrial applications. The implemented model also achieved high estimation accuracy and stability in various industrial tasks, being trained with the Free-space and Contact Data Sets.

One limitation with the current implementation that we foresee is the long time taken for large-scale data collection. Although the procedure is automatic, random-generated trajectories could be inefficient in covering the dynamic information of the robot. A systematic approach to generating trajectories

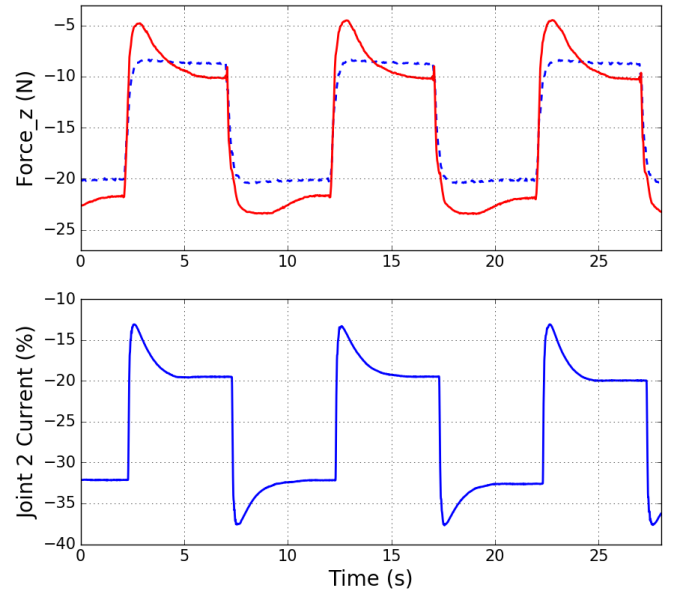


Fig. 10: Comparison between the true and estimated force with 0.1Hz force oscillation frequency. (a) Blue (dashed) and red lines indicate true and estimated force respectively, (b) the J2's current recorded simultaneously in force oscillation.

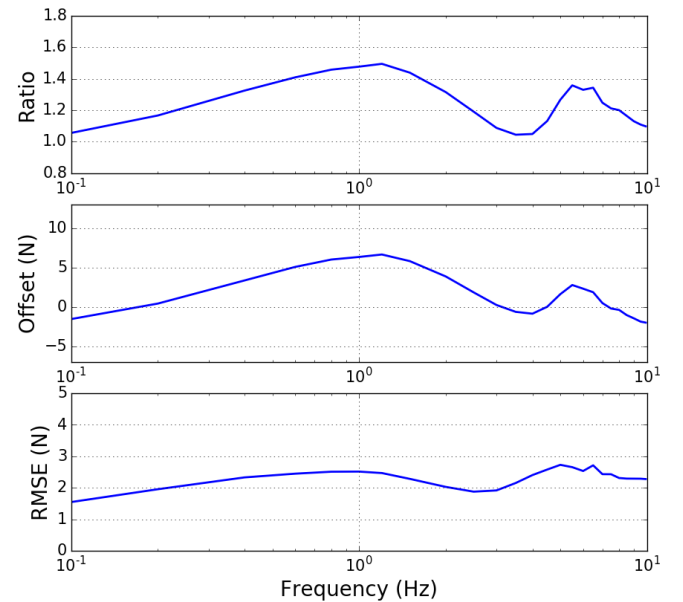


Fig. 11: The linear regression result of the mapping from true force to estimated force. Figures from top to bottom show (a) Gain (ratio) from true to estimated force, (b) mean error of between true and estimated force, (c) RMSE over all data at each frequency with force oscillation from 10N to 20N.

may significantly reduce the data collection time while allowing for higher accuracy.

All the experiments were carried out under low-speed operations – the most common mode for contact tasks. Further studies could be done to address the potential issues with high-speed operations. Such an improvement will allow accurate estimation in static and high-speed operations on which the



current model identification method shows less convincing results.

Since no dynamic information is required for model training, a similar method can be easily applied to different types of robot arms by following a standard data collection pipeline. The results in complex control tasks are also promising if the proposed method was applied in other areas like legged and surgical robots when a physical sensor was not preferred in actual applications.

Another promising avenue for future research is to combine the sensorless F/T estimation here with recent robust force control methods [3], which can further alleviate possible instabilities caused by estimation errors or delays. Such a combination could enable even more sensitive sensorless manipulation. From an economic perspective, the result presented here opens the possibility of equipping the existing 2.7 million industrial robots and the 600,000 new units installed per year with Force Sensing and Force Control capabilities without any additional hardware required for the users.

## VII. ACKNOWLEDGEMENT

This research was supported by the National Research Foundation, Prime Minister's Office, Singapore under its Medium Sized Centre funding scheme, Singapore Centre for 3D Printing, CES\_SDC Pte Ltd, and Chip Eng Seng Corporation Ltd.

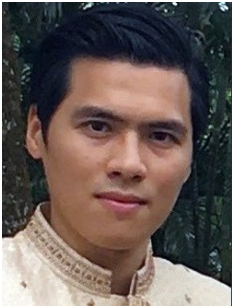
## REFERENCES

- [1] B. Siciliano, O. Khatib, and T. Kröger, *Springer handbook of robotics*, vol. 200. Springer, 2008.
- [2] F. Suárez-Ruiz, X. Zhou, and Q.-C. Pham, "Can robots assemble an ikea chair?," *Science Robotics*, vol. 3, no. 17, p. eaat6385, 2018.
- [3] H. Pham and Q.-C. Pham, "Convex controller synthesis for robot contact," *IEEE Robotics and Automation Letters*, vol. 5, no. 2, pp. 3330–3337, 2020.
- [4] A. De Luca and R. Mattone, "Sensorless robot collision detection and hybrid force/motion control," in *Proceedings of the 2005 IEEE international conference on robotics and automation*, pp. 999–1004, IEEE, 2005.
- [5] M. Van Damme, P. Beyl, B. Vanderborght, V. Grosu, R. Van Ham, I. Vanderniepen, A. Matthys, and D. Lefeber, "Estimating robot end-effector force from noisy actuator torque measurements," in *2011 IEEE International Conference on Robotics and Automation*, pp. 1108–1113, IEEE, 2011.
- [6] A. Wahrburg, J. Bös, K. D. Listmann, F. Dai, B. Matthias, and H. Ding, "Motor-current-based estimation of cartesian contact forces and torques for robotic manipulators and its application to force control," *IEEE Transactions on Automation Science and Engineering*, vol. 15, no. 2, pp. 879–886, 2017.
- [7] S. K. Kommuri, S. Han, and S. Lee, "External torque estimation using higher order sliding-mode observer for robot manipulators," *IEEE/ASME Transactions on Mechatronics*, vol. 27, no. 1, pp. 513–523, 2022.
- [8] D. Nguyen-Tuong and J. Peters, "Local gaussian process regression for real-time model-based robot control," in *2008 IEEE/RSJ International Conference on Intelligent Robots and Systems*, pp. 380–385, IEEE, 2008.
- [9] D. Nguyen-Tuong, M. Seeger, and J. Peters, "Model learning with local gaussian process regression," *Advanced Robotics*, vol. 23, no. 15, pp. 2015–2034, 2009.
- [10] A.-N. Sharkawy, P. N. Koustoumpardis, and N. Aspragathos, "Human-robot collisions detection for safe human-robot interaction using one multi-input-output neural network," *Soft Computing*, vol. 24, no. 9, pp. 6687–6719, 2020.
- [11] A. De Luca and R. Mattone, "Actuator failure detection and isolation using generalized momenta," in *2003 IEEE international conference on robotics and automation (cat. No. 03CH37422)*, vol. 1, pp. 634–639, IEEE, 2003.
- [12] N. M. Kircanski and A. A. Goldenberg, "An experimental study of nonlinear stiffness, hysteresis, and friction effects in robot joints with harmonic drives and torque sensors," *The International Journal of Robotics Research*, vol. 16, no. 2, pp. 214–239, 1997.
- [13] H. Olsson, K. J. Åström, C. C. De Wit, M. Gäfvert, and P. Lischinsky, "Friction models and friction compensation," *Eur. J. Control*, vol. 4, no. 3, pp. 176–195, 1998.
- [14] M. Ruderman, F. Hoffmann, and T. Bertram, "Modeling and identification of elastic robot joints with hysteresis and backlash," *IEEE Transactions on Industrial Electronics*, vol. 56, no. 10, pp. 3840–3847, 2009.
- [15] X. Liu, F. Zhao, S. S. Ge, Y. Wu, and X. Mei, "End-effector force estimation for flexible-joint robots with global friction approximation using neural networks," *IEEE Transactions on Industrial Informatics*, vol. 15, no. 3, pp. 1730–1741, 2018.
- [16] J. Hu and R. Xiong, "Contact force estimation for robot manipulator using semiparametric model and disturbance kalman filter," *IEEE Transactions on Industrial Electronics*, vol. 65, no. 4, pp. 3365–3375, 2017.
- [17] S. Schaal, C. G. Atkeson, and S. Vijayakumar, "Scalable techniques from nonparametric statistics for real time robot learning," *Applied Intelligence*, vol. 17, no. 1, pp. 49–60, 2002.
- [18] S. Vijayakumar and S. Schaal, "Local dimensionality reduction for locally weighted learning," in *Proceedings 1997 IEEE International Symposium on Computational Intelligence in Robotics and Automation CIRA'97: Towards New Computational Principles for Robotics and Automation*, pp. 220–225, IEEE, 1997.
- [19] A. Gijsberts and G. Metta, "Real-time model learning using incremental sparse spectrum gaussian process regression," *Neural networks*, vol. 41, pp. 59–69, 2013.
- [20] O. Sigaud, C. Salaün, and V. Padois, "On-line regression algorithms for learning mechanical models of robots: a survey," *Robotics and Autonomous Systems*, vol. 59, no. 12, pp. 1115–1129, 2011.
- [21] S. Lee and R. M. Kil, "Robot kinematic control based on bidirectional mapping neural network," in *1990 IJCNN international joint conference on neural networks*, pp. 327–335, IEEE, 1990.
- [22] L. H. Sang and M.-C. Han, "The estimation for forward kinematic solution of Stewart platform using the neural network," in *Proceedings 1999 IEEE/RSJ International Conference on Intelligent Robots and Systems. Human and Environment Friendly Robots with High Intelligence and Emotional Quotients (Cat. No. 99CH36289)*, vol. 1, pp. 501–506, IEEE, 1999.
- [23] H. Sadjadian and H. Taghirad, "Numerical methods for computing the forward kinematics of a redundant parallel manipulator," in *Proceedings of the IEEE Conference on Mechatronics and Robotics*, pp. 557–562, Citeseer, 2004.
- [24] N. Yilmaz, J. Y. Wu, P. Kazanzides, and U. Tumerdem, "Neural network based inverse dynamics identification and external force estimation on the da vinci research kit," in *2020 IEEE International Conference on Robotics and Automation (ICRA)*, pp. 1387–1393, IEEE, 2020.
- [25] M. Hanafusa and J. Ishikawa, "External force estimation for nonlinear systems using recurrent neural network," in *2019 IEEE/ASME International Conference on Advanced Intelligent Mechatronics (AIM)*, pp. 1055–1061, IEEE, 2019.
- [26] D.-H. Lee, W. Hwang, and S.-C. Lim, "Interaction force estimation using camera and electrical current without force/torque sensor," *IEEE Sensors Journal*, vol. 18, no. 21, pp. 8863–8872, 2018.
- [27] J. Xia and K. Kiguchi, "Sensorless real-time force estimation in microsurgery robots using a time series convolutional neural network," *IEEE Access*, vol. 9, pp. 149447–149455, 2021.
- [28] A. Marban, V. Srinivasan, W. Samek, J. Fernández, and A. Casals, "A recurrent convolutional neural network approach for sensorless force estimation in robotic surgery," *Biomedical Signal Processing and Control*, vol. 50, pp. 134–150, 2019.
- [29] D. Kim, D. Lim, and J. Park, "Transferable collision detection learning for collaborative manipulator using versatile modularized neural network," *IEEE Transactions on Robotics*, 2021.
- [30] M. A. Nielsen, *Neural networks and deep learning*, vol. 25. Determination press San Francisco, CA, USA, 2015.



**Shilin Shan** received the B.E. degree in Mechanical Engineering from Nanyang Technological University, Singapore in 2021. He is currently working towards the Ph.D. degree in Mechanical Engineering at the School of Mechanical and Aerospace Engineering, Nanyang Technological University, Singapore.

His research interests include robot manipulations and deep learning.



**Quang-Cuong Pham** was born in Hanoi, Vietnam. He is an alumnus of École Normale Supérieure, rue d'Ulm (France) and holds a Ph.D. in Neuroscience from Université Pierre et Marie Curie (France). He was a visiting researcher at the University of São Paulo (Brazil) in 2010, and a JSPS Fellow at the University of Tokyo (Japan) in 2011-2013. He joined NTU (Singapore) in 2013 and is currently

an Associate Professor in the School of Mechanical and Aerospace Engineering. He was a recipient of the Best Paper Award at the conference Robotics: Science and Systems, 2012. His research has featured in major international media, including The New York Times, The Guardian, The Economist, CNN, Science, Nature, etc. He is a Co-founder and Director of Eureka Robotics (<https://eurekarobotics.com/>), a deep tech startup devoted to solving the toughest automation challenges in manufacturing.

APPENDIX

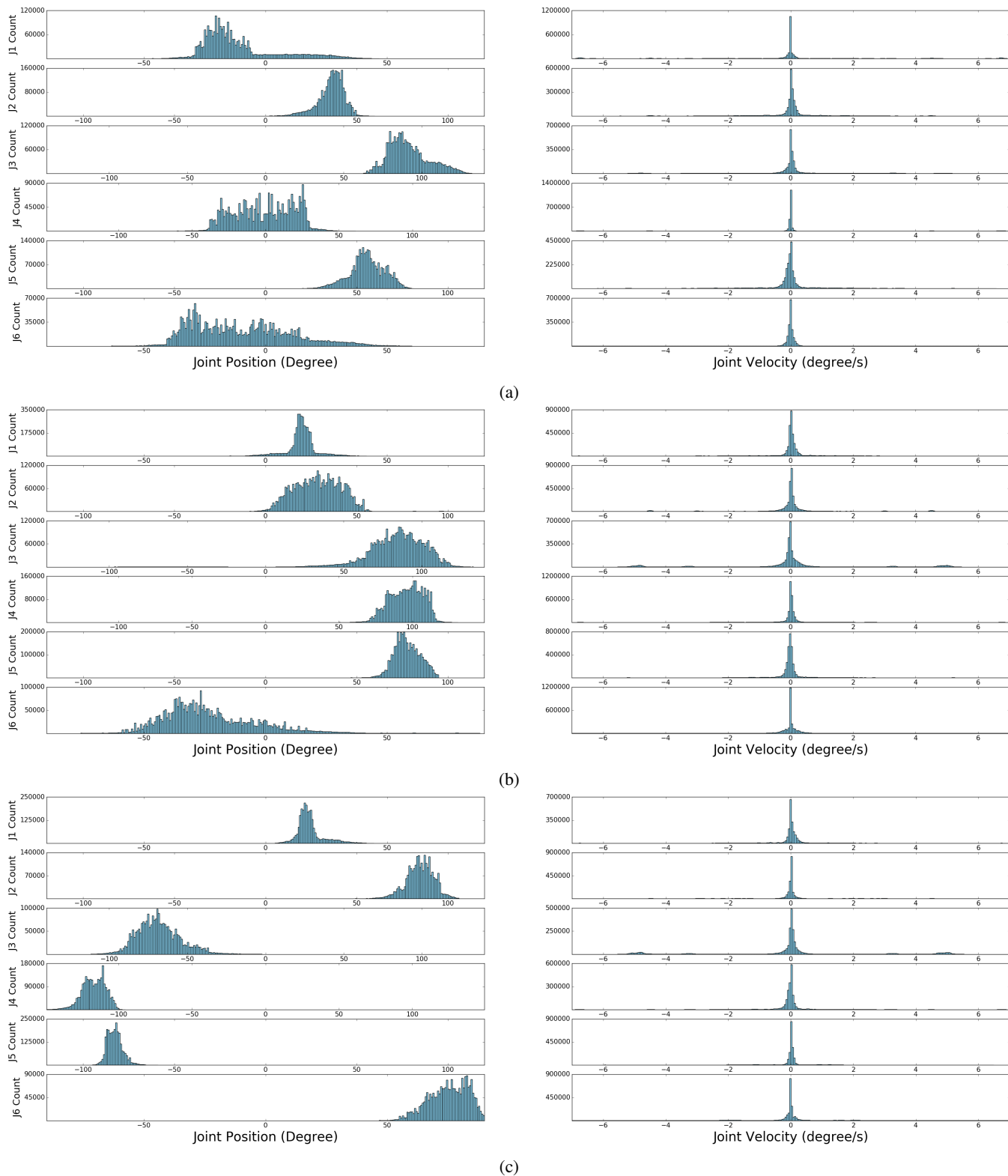


Fig. A.1: The joint-space training data distribution of joint positions and velocities for (a) IK1; (b) IK2; (c) IK3.

## LIST OF FIGURES

1	Pin insertion and hand-guiding snapshot . . . . .	1
2	Structure of MLP model . . . . .	3
3	Data set workspace and contact plane visualization . . . . .	4
4	Estimation and ground-truth comparison for free-motion . . . . .	5
5	Block diagrams for contact control . . . . .	6
6	Estimation and ground-truth comparison for spiral sliding . . . . .	6
7	Three-phase pin insertion algorithm visualization . . . . .	7
8	Estimation and ground-truth comparison for pin insertion . . . . .	7
9	Estimation and ground-truth comparison for hand-guiding . . . . .	7
10	Estimation and current measurement comparison . . . . .	8
11	Estimation error plotted against external force frequency . . . . .	8
A.1	Training data distribution visualization . . . . .	11

## LIST OF TABLES

I	Work-space and contact plane specifications for data sets . . . . .	4
II	Test set error . . . . .	5